Environmental Technology & Innovation 22 (2021) 101440

Contents lists available at ScienceDirect

Environmental Technology & Innovation

journal homepage: www.elsevier.com/locate/eti

Hydropyrolysis of freshwater macroalgal bloom for bio-oil and biochar production: Kinetics and isotherm for removal of multiple heavy metals

Krishna Kumar Jaiswal [a], Vinod Kumar [a,b,c,*], Mikhail S. Vlaskin [d], Manisha Nanda [e], Monu Verma [f,**], Waseem Ahmad [a], Hyunook Kim [f,**]

[a] Algae Research and Bioenergy Laboratory, Department of Chemistry, Uttaranchal University, Dehradun, Uttarakhand, 248007, India
[b] Peoples' Friendship University of Russia (RUDN University), Moscow, 117198, Russia
[c] Department of Environmental Monitoring and Forecasting, Ecological Faculty, RUDN University, Moscow, 117198, Russia
[d] Joint Institute for High Temperatures of the Russian Academy of Sciences, 13/2 Izhorskaya St, Moscow, 125412, Russia
[e] Department of Biotechnology, Dolphin (P.G.) Institute of Biomedical and Natural Sciences, Dehradun, Uttarakhand, 248007, India
[f] Water-Energy Nexus Laboratory, Department of Environmental Engineering, University of Seoul, Seoul, 02504, Republic of Korea

ARTICLE INFO

Article history:
Received 24 November 2020
Received in revised form 13 February 2021
Accepted 13 February 2021
Available online 17 February 2021

Keywords:
Hydropyrolysis
Heavy metal ions
Kinetics and isotherm
Algal blooms
Bio-char and bio-oil

ABSTRACT

In this study, hydropyrolysis was carried out using sodium carbonate to convert the green algal bloom into bio-oil, biochar, aqueous solution, and gases. The effect of supercritical conditions (400, 450, 500 °C) on the product yield, bio-oil composition, and structure, and functionalities of the biochar was determined. The high yield of biochar and bio-oil was reported at 400 °C. A significant reduction in bio-oil and increment in hydrocarbon content was reported on the elevation of temperature from 450 °C to 500 °C. After that, kinetic and isotherm analysis was investigated simultaneously to remove four heavy metals viz. Cu(II), Ni(II), Co(II), and Cd(II) from the mixture solution. Results show that kinetics data follow a pseudo-second-order kinetics model and adsorption isotherm is in better agreement with the Langmuir model, not with the Freundlich model. The maximum adsorption capacity was found 10.90, 5.74, 5.80, and 16.28 mg/g with the biochar prepared at 500 °C for Cu(II), Ni(II), Co(II), and Cd(II) metals, respectively. The current investigation provided a promising way for the utilization of freshwater algal bloom biomass for renewable products and simultaneously heavy metal removal from the water.

1. Introduction

Marine and freshwater microalgae are essential components of the water ecosystem and a good source of biomass (Bird et al., 2011). Macroalgae are multicellular organisms approximately growing up to 60 m in freshwater (Demirbas and Fatih, 2010). Macroalgal biomass is a good source of biologically active compounds like chemicals, nutraceuticals, food, feed, fertilizers, etc.

* Corresponding author at: Algae Research and Bioenergy Laboratory, Department of Chemistry, Uttaranchal University, Dehradun, Uttarakhand, 248007, India.
** Corresponding authors.
E-mail addresses: vinodkdhatwalia@gmail.com (V. Kumar), mkvcyiitr@gmail.com (M. Verma), h_kim@uos.ac.kr (H. Kim).

https://doi.org/10.1016/j.eti.2021.101440
2352-1864/

The excessive growth of green macroalgae resulted in macroalgal bloom or tide events in the world (Morand and Merceron, 2005; Merceron et al., 2007). Accumulation of algal blooms in freshwater rivers and ponds leads to low dissolved oxygen and microbial decomposition (Kumar et al., 2019). On the other hand, biomass from microalgae cultivation systems for wastewater treatment has also shown potential to be recycled for the preparation of bio-chars and bio-oils (Li et al., 2018a,b,c, 2020a,b,c; Jaiswal et al., 2021). Recently several processes have been proposed for the transformation of biomass into bio-crude oil, gas and biochar. Fast pyrolysis based on a high temperature and pressure is the most promising one (Li et al., 2018a,b). One of the solutions for the management of macro-algal biomass is pyrolysis in which feedstock is decomposed into biochar, bio-crude oil, and gas under limited O_2 conditions and temperature range 300–800 °C (Kumar and Nanda, 2016; Yu et al., 2017).

Unlike the traditional pyrolysis method, hydropyrolysis can be operated at moderate temperatures, utilizing whole algal biomass to produce a high yield of bio-oil, biochar, organic acid rich aqueous and gases (Zhou et al., 2013; Chiaramonti et al., 2017). In the hydropyrolysis process, bio-oil formed with better quality and with low O_2 content (Zhou et al., 2013). Also, the addition of catalyst (e.g. Na_2CO_3) in hydropyrolysis processes proliferates the evolution of bio-chars and bio-oils (Jaiswal et al., 2021). The effect of the hydropyrolysis process catalyzed with Na_2CO_3 and non-catalytic has already been reported in the literature (Shakya et al., 2015).

Recently, urbanization and industrialization have led to the problem of mixed heavy metal pollution which is a major cause of concern for the management of water resources and the environment. This problem has gained the attention of researchers who are striving to provide an efficient and appropriate technique to mitigate mixed heavy metal pollution (Li et al., 2020a,b,c; Ren et al., 2020).

Various physical and chemical processes like salting out, coagulation, ion exchange, osmosis process, ultrafiltration, and adsorption are employed on an industrial scale to mitigate heavy metals from the wastewaters (Fu and Wang, 2011). Inappropriately, the above said technologies are considered by costly disposal, high energy-consuming, generation of massive sludge, low selectivity, etc. This thereby increases the wastewater treatment cost (Fu and Wang, 2011).

Adsorption is a relatively new and cheap process providing flexibility to design (Li et al., 2019). It is a reversible and naturally adaptable alternative that can be used under different environmental conditions to remove heavy metals from wastewaters (Wang and Chen, 2009; Park et al., 2010). Many types of waste material or organic waste have been reported to be utilized in the mitigation of heavy metal from polluted water (Gupta et al., 2015; Carolin et al., 2017). These waste materials do not act as good absorbents for industrial effluent treatment due to their moderate adsorption capacity and their requirements in large amounts (Gupta et al., 2015). Hence researchers have used many technologies to improve the performance of low-cost material (Bird et al., 2011).

Algae biochar is considered by low volatile carbon constituents and small surface area but is high in inorganic nutrients like Ca, K, Mg, and P, which make it suitable as a fertilizer. Algal biochar can be used in other applications like the source of energy or as an absorbent for removal of micropollutants (Bird et al., 2011; N'Yeurt and Iese, 2015; Cole et al., 2017; Yu et al., 2017; De Bhowmick et al., 2018).

In this study, freshwater macroalgal blooms were used as feedstock for the preparation of biochar by the hydropyrolysis method. By this process, bio-oil and biochar have been obtained. The biochar was used to adsorb heavy metals from mixed metal solution. This study achieves dual-purpose (I) production of bio-oil and (II) the mitigation of mixed heavy metal from the wastewater to protect the environment.

2. Materials and methods

2.1. Sample preparation

Macro-algal bloom was acquired from a freshwater river near University (30°20′31.9016″N 77°57′16.3162″E) during the month of Jan–Feb (2019). The raw biomass was cleaned with DI water and sun-dry for 3–5 days, then powered into <2.0 mm particle size. The proximate analysis was done according to the Association of Official Analytical Chemists (AOAC) methods. Carbon, hydrogen, sulfur, and nitrogen composition were analyzed via an elemental analyzer (Thermo Fisher, USA).

The pyrolysis process was carried out in batch mode in three custom-made 50 ml stainless steel (SS-316) reactors. Muffle furnace (ACMAS Technologies Pvt-Ltd) was used for heating (rate 5–10/min). The operating temperature employed in this study was supercritical conditions (400–500 °C). To start the experiment, the reactor was charged with water and biomass ratio 6:1 and catalyst ratio 1:10 Na_2CO_3. This ratio was selected in accordance with our prior study (Kumar et al., 2019), which suggested the maximum bio-oil production from macroalgae. The use of alkaline catalyst is recommended for high yield, improving pH, and quality of bio-crude oil (Ross et al., 2010; Jena et al., 2012).

2.2. Product separation

Subsequently, the retention time reactor was cooled, gaseous products were vented off, and the liquid phase and solid phase were separated. In the liquid phase, dichloromethane was added and the filtrate upper layer was separated from the aqueous layer. The solvent present in the upper layer was evaporated, and the remaining residue was collected and noted as Bio-oil-1. Solid-phase was treated three times with acetone for the separation of acetone-soluble bio-oil. Acetone

Table 1
Biocrude oil and biochar yields under supercritical conditions.

Temperature	Biocrude oil	Biochar
400 °C	15.8%	61.6%
450 °C	12.3%	58.8%
500 °C	11.6%	55.1%

was evaporated, and bio-oil received mixed with bio-oil-1 and was weighed. The solid residue was obtained and then washed with DM (demineralized) water. Subsequently, it was dried at 55 °C and marked as biochar. Biochar was ground into 0.75–1.00 mm powder for further study. Bio-oil and biochar obtained at 400 °C, 450 °C, and 500 °C are marked as BO-4, BC-4, BO- 4.5, BC-4.5, BO-5, and BC-5, respectively. The bio-oil and biochar yield was calculated using the following equation:

$$Bio-oil\,(\%) = \frac{Organic\ fraction}{Dry\ weight\ of\ algae} \times 100 \tag{1}$$

$$Bio-char\,(\%) = \frac{Solid\ phase}{Dry\ weight\ of\ algae} \times 100 \tag{2}$$

2.3. Qualitative characteristic of bio-oil and bio-char

The constituents of bio-oil products were evaluated by GC–MS (GC–MS; Agilent Technologies, USA) (Kumar et al., 2019). The morphologies of biochar were evaluated using FESEM (Quanta 200 FEG). The functional groups attached with biochars were detected using Fourier transform infrared spectroscopy at ATR mode (ATR-FT-IR, Termo Nicolet Model: 6700) at spectra 400–4000 cm^{-1}. The crystalline structure of the biochar was studied by XRD (Bruker, Model: D8 ADVANCE ECO) in the 2θ range 20–80°. Specific surface area and pore structure of biochar were determined by the Emmette–Teller (BET) system of N_2 adsorption isotherms at 77.35 K (Micrometrics Instruments USA-ASAP2020). The structural evaluation of the biochar was determined at an excitation wavelength of 785 nm by Raman Spectroscopy (RENISHAW in Via Raman confocal microscope system).

2.4. Application of biochar in heavy metals adsorption

The experiments for batch adsorptions were investigated at the temperature of 25 °C. The mixture heavy metal solution was prepared by dissolving Ni(II) (10 mg/L), Co(II) (10 mg/L), Cd(II) (30 mg/L), and Cu(II) (20 mg/L) salts in deionized water to make the final volume of metal 70 mgL^{-1}. The presence of the aforementioned heavy metals has generally been observed in raw urban wastewater, as reported in our previous study (Arora et al., 2020). We have chosen the content of heavy metals in relation to the occurrence in urban wastewater and also in accordance with the literature (Jaiswal et al., 2021). Approximately 0.250 g of biochar was mixed into 100 ml of heavy metals solution of pH-5 in a 250 ml. The conical flask was then placed on a rotatory shaker (150 rpm) for 24 hr. After 24 hr solution was separated by centrifuge from the mixture and then, the liquid phase was again elucidated by a 0.20 μm syringe filtration. The remaining concentration of the metal ion was evaluated by ICP-MS (Jaiswal et al., 2021). The adsorptions of different heavy metal by biochar was represented in removal efficiency and adsorption capacity (q_e) and calculated by the following equations

$$Removal\ efficiency\,(\%) = \left(\frac{C_0 - C_e}{C_0}\right) \times 100 \tag{3}$$

$$\text{Adsorption capacity}\ (q_e) = (C_o C_e) \times \frac{V}{m} \tag{4}$$

Where C_o and C_e are initial and equilibrium concentrations of metal ions, respectively, while V (ml) and m (mg) are the volumes of solutions and weight of the used adsorbent.

2.5. Statistical analysis

The hydropyrolysis reaction and adsorption experiment was conducted in triplicate, and descriptive statistics acquired the standard deviation.

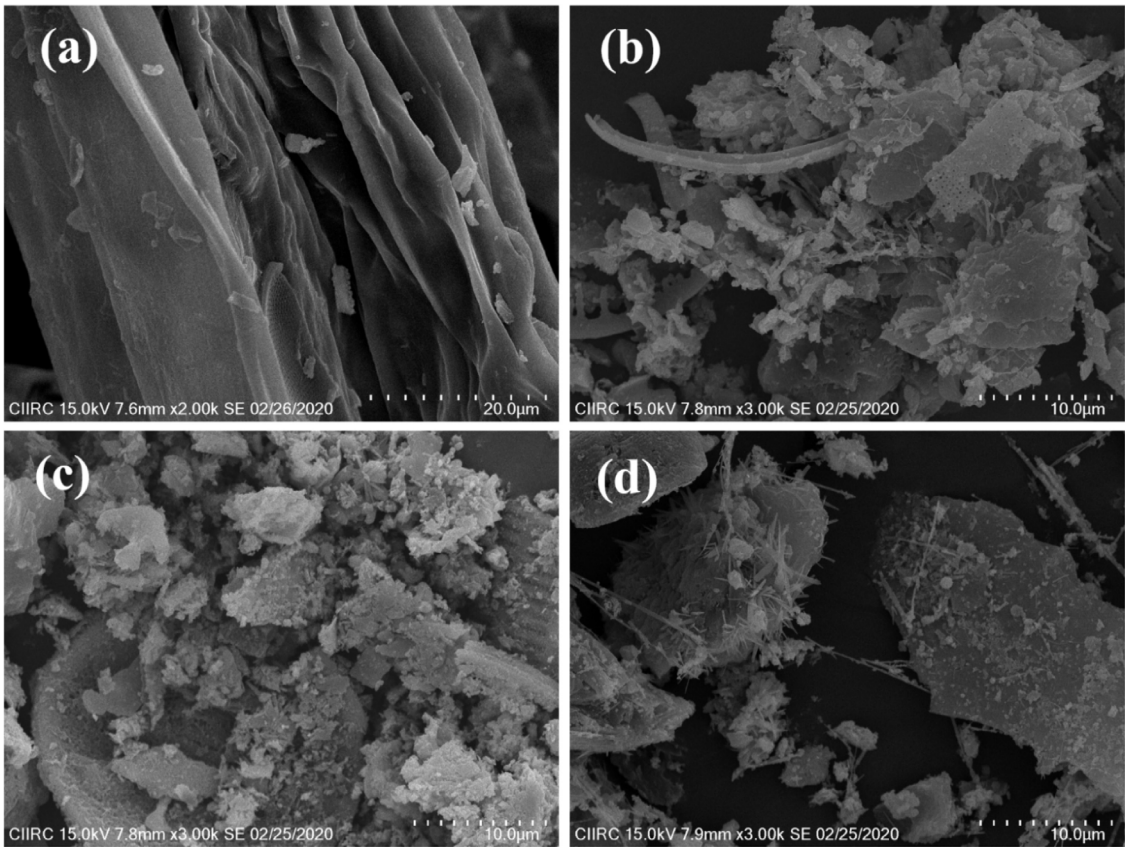

Fig. 1. FESEM images and EDS spectra of (a) Biomass, (b) BC-4, (c) BC4.5 and (d) BC-5.

3. Results and discussion

In this investigation, the macroalgal bloom was utilized as hydropyrolysis feedstocks at supercritical temperature (400 °C to 500 °C). The reaction was carried out for 30 min with a Na_2CO_3 catalyst. Temperature change displayed a substantial effect on biochar and bio-oil yields as presented in Table 1. Among all physical parameters, hydropyrolysis temperature plays an important role in product composition and yield as reported (Garcia Alba et al., 2012).

The proximate and elemental analysis of algal biomass gives the following constituents such as 89.14% moisture, 69.31 ± 2% volatile solids, 30.69 ± 4% ash content, 14.91% C, 1.73% N, 1.66% H and 1.19 S, respectively.

Results show that hydropyrolysis bio-oil yields decreased with a rise in reaction temperature from 400–500 °C. Ross et al. (2019) described the highest yields of bio-crude oil at 350 °C (Ross et al. 2019). Chen et al. described 49.9% of bio-oil yield at 300 °C (1 hr) from mixed macro and microalgal biomass (Chen et al., 2014a,b). Hydrothermal product yield depends on the type of biomass composition, catalysts, retention time, and temperature (Jena et al., 2012). The molecular constituent of the bio-oil was evaluated by GC–MS. The identified compound is reported in Table 2. The recognized organic compounds were categorized into the following types: ketones/aldehydes, phenols, alcohol, hydrocarbons, and organic acids. Their relative amount varied with a temperature change, as shown in Table 1. It was observed that 400 °C bio-oil contains a high content of fatty acid, while the composition of hydrocarbon content enhances with a rise in operating temperature. The higher temperature is reported to convert the fatty acids into hydrocarbon (Choudhary et al., 2017).

In this study, an upsurge in temperatures from 400 to 500 °C leads to a decrease in the yields by 7.5%. This reduction in yield may be due to loss of volatile and condensation of aliphatic compounds (Lam et al., 2012). Selvanathan et al. and Dai et al. also described a decrease of biochar yield with a rise in temperature (Dai et al., 2013; Selvanathan et al., 2017).

FESEM was used to analyze the structural morphology of biomass and biochar. Fig. 1 shows the FESEM images of biomass and biochar. The surface morphology of the biochar prepared from the macroalgae biomass revealed a mutilated shape and a distorted surface due to the volatilization of organic components and thermal pyrolysis. Biochar has been observed for the formation of structures such as flakes and needles including spherical and oval structures. The irregular flakes like structure were generated at high temperature due to the condensation of organic hydrocarbon materials such as tars and the successive disintegration of carbonization products. This suggested that the hydropyrolysis process damaged

Table 2
Major compounds identified by GC–MS in hydropyrolysis bio-oil at different temperatures.

Compound name	Area%			Category
	400 °C	450 °C	500 °C	
3-Penten-2-one, 4-methyl	4.4	13.2	15.2	Ketones/aldehydes
2-Pentadecanone, 6,10,14-trimethyl	18.3	6.2	–	Ketones/aldehydes
9-Hexacosene	8.6	11.5	20.2	Hydrocarbons
11,15-Tetramethyl-2-hexadecene	–	–	7.1	Hydrocarbons
Heptadecyloctanoate		2.8	1.4	Esters
Phytol	10.3	8.6	9.2	alcohol
2-Methyl-2-hexanol	2.7	–	1.3	alcohol
Tetradecanoic acid	2.7	1.4	–	Fatty acid
n-Hexadecanoic acid	15	10	8	Fatty acid
Pentadecanoic acid	19.2	1.2	–	Fatty acid
Phenol	5.8	8.4	7.1	Phenol

Table 3
FTIR spectral band of biomass and biochar with functional group.

Wave numbers (cm^{-1})	Functional groups/Assignments	Biomass	Biochar		
			400 °C	450 °C	500 °C
3200–3700	O–H Stretching Acid, methanol	3354	–	–	–
2800–3000	C–H_n stretching, Alkyl, aliphatic, aromatic	2932, 2509	2932, 2509	2932, 2509	2932, 2509
1750–1630	C=O Stretching, Ketone, Ester, Amide	1653	1675	1675	1675
1470–1430	O–CH3 stretching, Methoxyl–O–CH_3	1425	1425	1425	1425
1440–1400	OH, bending Acid	1425	1425	1425	1425
1000–1200	C=O/C-O-C	1101, 1176	1101, 1155	–	1101
750–870	C–N/R-O-C/R-O-CH_3 stretching aromatic C–H	711, 797, 873	711, 797, 873	711, 797, 873	711, 797, 873
700–400	C–C stretching	461	613, 461	613, 461	613, 461

and altered the smooth arrangement into aromatic compounds (Li et al., 2017). The EDX spectroscopy of the biomass and biochars are displayed in Fig. 1S (supplementary information).

FTIR examination was performed for functional group identification existing in the biochar. The adsorption spectra of biochar and biomass are shown in Fig. 2 and the wavenumber and vibrational mode recorded in Table 3. The peak at 3354 cm^{-1} ascribed to the O–H stretching and peaks at 1653, 1036, 1155 cm^{-1} ascribes to the C=O stretching endorses the attendance of the carboxyl groups. Zhao et al. reported that carboxyl acid groups on biochar showed functional adsorption capability of heavy metals (Zhao et al., 2019). Further decrease in the strength of the peak at 3354 cm^{-1} (O–H) and 1653 cm^{-1} (C=O), probably due to an increase in temperature during hypothermal conditions, lead to loss of functional groups in biochar.

Raman spectra were determining the structure of biochar and biomass. The result of the region 250–2000 cm^{-1} is shown in Fig. 3. Raman spectra of biochar consist of two main bands: G band (1560–1610 cm^{-1}) and D band (1320–1380 cm^{-1}). The D band represents the amorphous graphite or distorted sp^2 hybridized carbon atom, while the G band is related to the incidence of graphite crystallites. The graphitic degree of carbon was calculated by the ratio of I_D/I_G (McDonald-Wharry et al., 2013). A high I_D/I_G ratio was reported in the biochar obtained at 500 °C. An upsurge in the I_D/I_G ratio was stated with an increase in the hydropyrolysis temperature. A similar change in G and D band was reported by Maliutina et al. (2018) in microalgal biochar (Maliutina et al., 2018). An increase in I_D/I_G value with a rise in pyrolysis temperature from 300–600 °C was also reported by Rhim et al. (2010).

The XRD of biochar is presented in Fig. 4. The shape peaks between 30–60 show the presence of calcinating, rutile, Fe_3O_4, and FeS minerals (Fan et al., 2015). The sharpness of peak intensifications with a rise in the hydropyrolysis temperature might be due to the destruction of the ultrastructure of algal biomass. The surface area of biochar increases 2.70 to 3.98 m^2/g with the rise in temperature 400−500 °C and the values are listed in Table 4. A similar biochar surface area (1.0482) was reported by Jung et al. in marine macroalgae (Jung et al., 2015). Breakdown of ester groups and aliphatic alkyl at high temperatures leads to proliferation in the surface area of biochar (Jung et al., 2013).

3.1. Effect of contact time for heavy metals removal and adsorption kinetics

In this part, the effect of contact time was performed to find out the equilibrium between the adsorbent and heavy metal ions. For this purpose, initial concentrations of the Cu(II) (20 mg/L), Ni(II) (10 mg/L) Co(II) (10 mg/L) and Cd(II) (30 mg/L) metal ions were used. The biochar and the mixture of the heavy metal ions were dispersed in the shaker and permitted to contact at varied intervals time. Fig. 5 displays the kinetic curve for the different metal ions which indicates that the adsorption was fast in the initial 180 min and the maximum amount of the metal ions were adsorbed to reach a plateau after the contact time of 240 min. In an investigation, the maximum adsorption capacity of 42 mg/g of Cd(II) has been examined from the aqueous solutions at 25 °C for 120 min by using dry waste biofilms. They have suggested

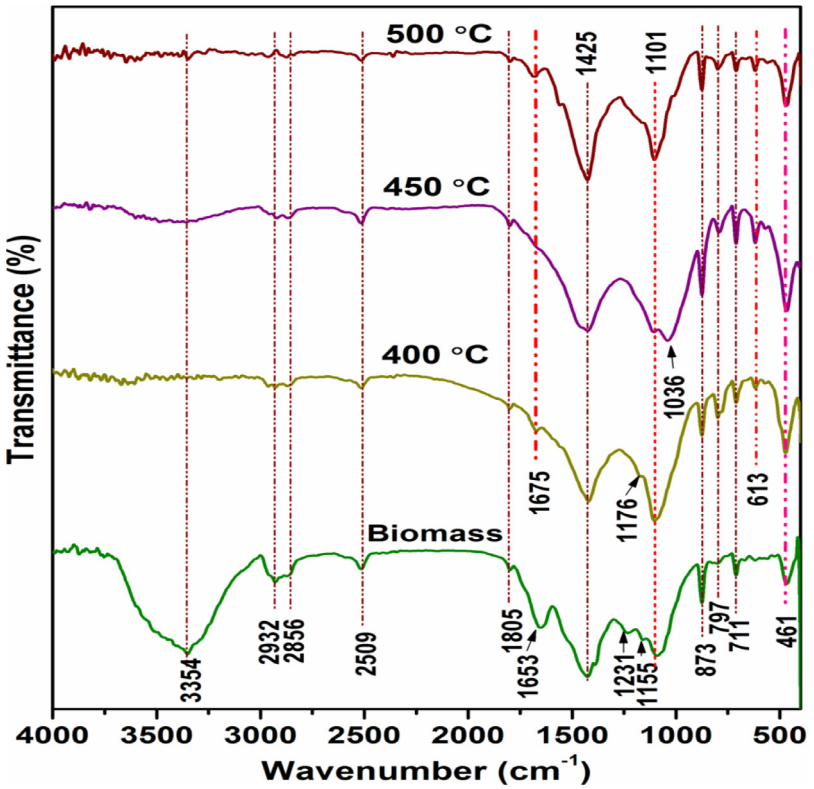

Fig. 2. ATR-FTIR spectra of biomass and prepared biochar (BC) at various temperatures.

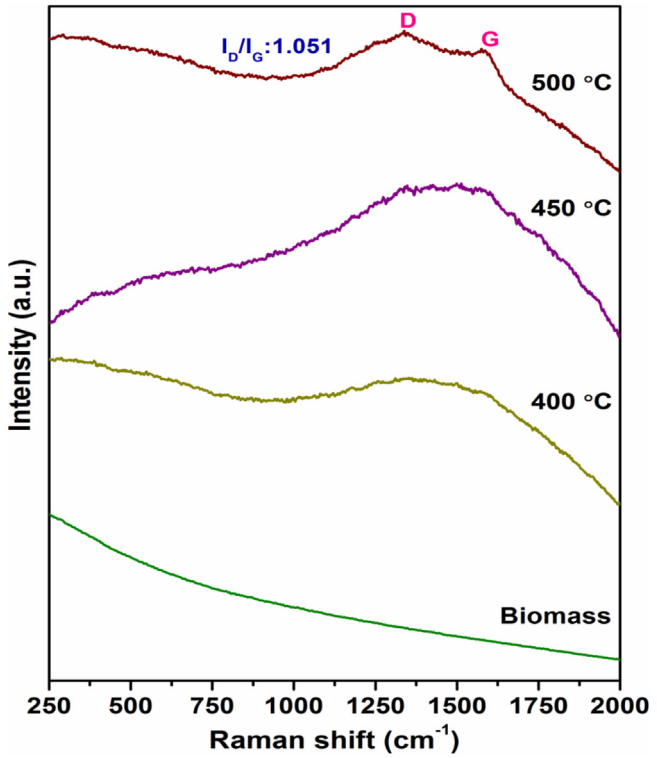

Fig. 3. Raman spectra of biomass and prepared biochar (BC) at various temperatures.

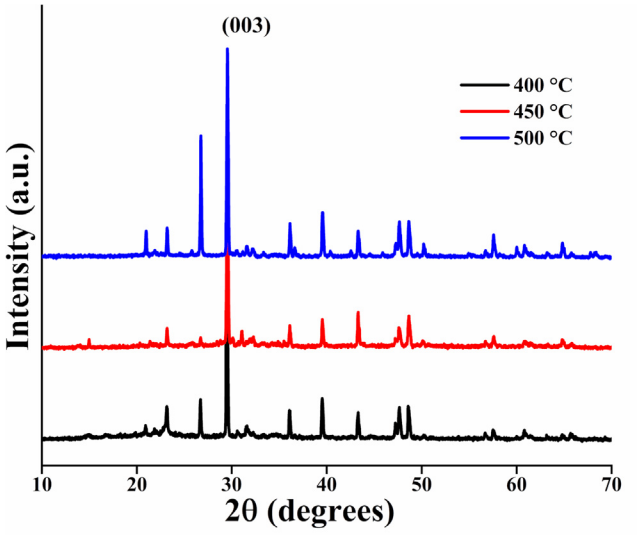

Fig. 4. X-ray diffraction spectroscopy (XRD) of prepared biochar (BC) at various temperatures.

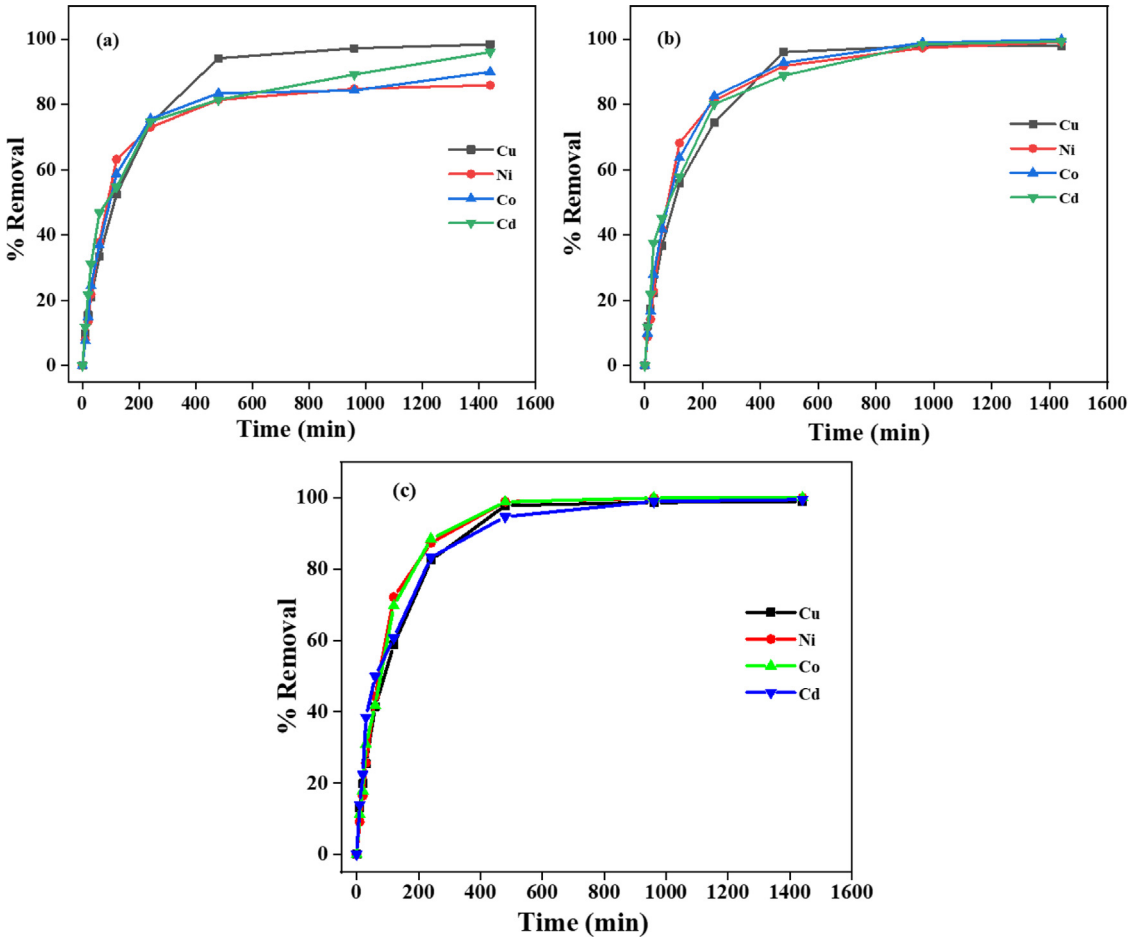

Fig. 5. Percentage removal of Cu (II), Ni (II), Co (III) and Cd (II) metal ions from the multiple-metal system by algae biochar prepared at (a) 400 °C (b) 450 °C, and (c) 500 °C. Initial pH =5, adsorbents dose = 250 mg/L, and initial metal ions concentration were 20, 10, 10 and 30 mg/L, and 250 mg, respectively.

Table 4
Biochar surface area and effect on mixed heavy metal solution pH.

Biochar	BET surface area	Change in pH by mixing biochar
400 °C	2.70	6.1
450 °C	4.06	6.8
500 °C	3.98	7.5

Table 5
Pseudo-first-order and Pseudo-second-order kinetics parameters for different multiple heavy metal ions onto algae biochar prepared at different temperatures (a) 400° C, (b) 450° C and, (c) 500° C.

System (a) 400 °C	Pseudo-first-order			Pseudo-second-order		
	q_e (mg g^{-1})	k_1(min^{-1})	R^2	q_e (mg g^{-1})	k_2 (g mg^{-1} min^{-1})	R^2
Cu	104.02	0.0048	0.966	9.09	0.001	0.998
Ni	60.94	0.0046	0.936	3.70	0.003	0.997
Co	59.73	0.0030	0.779	3.84	0.003	0.997
Cd	127.94	0.0026	0.89	12.5	0.001	0.998
System (b) 450 °C	Pseudo-first-order			Pseudo-second-order		
	q_e (mg g^{-1})	k_1(min^{-1})	R^2	q_e (mg g^{-1})	k_2 (g mg^{-1} min^{-1})	R^2
Cu	221.38	0.0072	0.992	9.86	0.001	0.998
Ni	125.85	0.0042	0.953	4.34	0.002	0.998
Co	143.42	0.0048	0.983	4.29	0.002	0.999
Cd	322.25	0.0042	0.986	14.28	0.0008	0.999
System(c) 500 °C	Pseudo-first-order			Pseudo-second-order		
	q_e (mg g^{-1})	k_1(min^{-1})	R^2	q_e (mg g^{-1})	k_2 (g mg^{-1} min^{-1})	R^2
Cu	307.72	0.0066	0.955	11.25	0.001	0.999
Ni	213.85	0.0073	0.978	5.28	0.002	0.997
Co	205.42	0.0095	0.982	5.10	0.003	0.997
Cd	612.25	0.0055	0.989	17.24	0.001	0.999

that the removal efficiency of Cd(II) extended 89.3% when the dose of biosorbent was 2.0 g/L (He et al., 2018). The initial higher rate due to the accessibility of exposed surface area of the adsorbents as the adsorption kinetics can be influenced by the surface area of the adsorbent. Also, kinetics removal shows the higher and faster to remove heavy metals ions by biochar achieved at a higher temperature compared to lower temperature-based biochar. As per the literature survey, high pyrolysis temperature leads to improved surface area and porosity in comparison to the original biomaterials (Fig. 1 and Table 4). Higher surface area and porosity can increase the adsorption of metal ions (Tan et al. 2014). The higher temperature of pyrolysis also upsurges the concentration of the minerals (i.e. K, Ca, Mg, and P) on the sorbent's surfaces to be employed for the exchange of heavy metal ions (Hossain et al., 2011; Subedi et al., 2016; Zhao et al., 2019).

Kinetic modeling has been carried out to observe the rate of adsorption of heavy metal ions and the evidence of heavy metal adsorption mechanisms on bio-char materials. To describe the adsorptions, two different kinetic models which are pseudo-first-order (PFO) and pseudo-second-order (PSO) models, were usually applied. These models adopt the adsorption rate of heavy metal ions on the surface of materials is proportionate to the number of vacant sites. PFO kinetic model is controlled by the physical procedure, while PFO kinetic is precise by chemical procedures, comprising valence forces that share or exchange electrons among the adsorbent and adsorbate. The mathematical form of the PFO and PSO kinetic models were represented by Eq. (4) and (5), respectively (Verma et al., 2017, 2020)

$$\ln(q_e - q_t) = \ln q_e - k_1 t \tag{5}$$

$$\frac{t}{q_t} = \frac{1}{k_2 q_e^2} + \frac{t}{q_e} \tag{6}$$

Where q_e and q_t are the metal ion adsorbed amounts (mg/g) at equilibrium, and at time t, respectively, and k_1 and k_2 are the rate constant of the adsorption of first and second orders, respectively. The results of PFO and PSO parameters were displayed in Table 5 and Fig. S(2–4). From the kinetics modeling data, it is marked that the values of the regression coefficient (R^2) for the PFO model did not fit well but fit well with the PSO model for all metals, indicating the chemical adsorption process of heavy metal ions on the adsorbent's surface by valence forces share or exchange electrons among the adsorbent and adsorbate.

3.2. Effect of metal ions concentration and isotherm models

The effect of initial concentrations to remove metal ions were investigated by taking the concentration range from 10 ppm to 300 ppm at optimum pH and room temperature conditions, and the result is demonstrated in Fig. 6. Data

Table 6
Fitting parameters of Langmuir and Freundlich isotherm models for different multiple heavy metal ions onto algae biochar prepared at different temperatures (a) 400 °C, (b) 450 °C and, (c) 500 °C.

System (a) 400 °C	Langmuir			Freundlich		
	q_m (mg g^{-1})	K_L(L mg^{-1})	R^2	K_F (mg g^{-1})	n	R^2
Cu	8.33	0.50	0.999	4.30	1.81	0.962
Ni	3.89	0.61	0.998	2.88	3.44	0.935
Co	4.50	0.31	0.994	2.65	5.28	0.950
Cd	12.5	0.16	0.999	7.84	2.77	0.977
System (b) 450 °C	Langmuir			Freundlich		
	q_m (mg g^{-1})	K_L (L mg^{-1})	R^2	K_F(mg g^{-1})	n	R^2
Cu	9.42	0.58	0.994	6.76	3.42	0.947
Ni	4.54	0.66	0.997	3.87	2.86	0.957
Co	4.82	0.29	0.993	3.93	2.56	0.979
Cd	14.61	0.88	0.999	7.46	2.56	0.968
System (c) 500 °C	Langmuir			Freundlich		
	q_m (mg g^{-1})	K_L(L mg^{-1})	R^2	K_F (mg g^{-1})	n	R^2
Cu	10.90	0.73	0.998	4.30	2.10	0.965
Ni	5.74	0.56	0.996	3.97	6.90	0.913
Co	5.80	0.66	0.996	3.70	8.40	0.960
Cd	16.28	0.78	0.998	8.67	3.84	0.921

indicates that the percentage of heavy metal ion removal was high at lesser concentration and continuously decreased by the elevation of the equilibrium concentration of a metal ion in the solution. The removal efficacy was not extensively decreased when the equilibrium concentration of metal ion achieved 100 mg/L, indicating the available sites for adsorption has been reached at saturation. When a concentration of the metal ion was < 50 mg/L, the removal efficiency was sufficient which indicates that for less concentration was plentiful blank adsorption sites available in the used biochar. When the metal ions concentration was 50–300 mg/L, the removal efficacy was slower which shows the deficiency of effective adsorption sites in the used biochar, which limited the decrease in the removal efficiency. Also, data indicates the higher removal efficiency with the biochar prepared at 500 °C, indicating the more available effective adsorption sites biochar compare to prepare at lower temperature.

The data observed in the adsorption process was fitted to two famous isotherm models; Langmuir and Freundlich isotherms to define the equilibrium relationship between adsorbate and adsorbent at dynamic equilibrium. The linear form of the Langmuir (Langmuir, 1918) isotherm model is designated as follows:

$$\frac{C_e}{q_e} = \frac{1}{K_L q_m} + \frac{C_e}{q_m} \tag{7}$$

Where q_e is the equilibrium adsorption capacity (mg/g), q_m is the largest Langmuir adsorption capability corresponding to the integral single-deck enshroud (mg/g), C_e is the concentration (mg/L) at equilibrium, and K_L is the Langmuir adsorption constant associated with the rate of adsorption (L/mg). The q_m and K_L values can be calculated by intercept and slope from the linear fitting of C_e/q_e versus C_e.

The linear form of Freundlich isotherm (Freundlich, 1907) model is expressed as

$$lnq_e = lnK_F + \frac{1}{n} lnC_e \tag{8}$$

Where K_F and n are the Freundlich constants associated with the adsorption capacity and degree of system heterogeneity, respectively. The value of K_L and q_m can be calculated by intercept and slope from the linear fitting of C_e/q_e versus C_e.

The linear fitting parameters of Langmuir and Freundlich isotherms with different biochars are listed in Fig. S(5–7) and Table 6. Data indicated that the correlation coefficient (R^2) fit well with the Langmuir isotherm model, not with the Freundlich isotherm model, demonstrating the monolayer adsorption. The results of the higher adsorption capacity with all heavy metal ions are listed in Table 6. In a similar study, (Jaiswal et al., 2021) have also investigated kinetic and isotherm analysis to understand the different adsorption behaviors of bio-char in multiple heavy metal solutions, viz. Cu (II), Ni (II), Co (III) and Cd (II). Pseudo second order kinetics model and Langmuir's model fitted well for kinetics and adsorption isotherms, respectively. The relative adsorption capacities of different types of bio-chars are shown in Table 7.

3.3. Effect of pH for heavy metals removal

Solution pH is an important parameter in the adsorption process that is affected by the surface charge and function group on the adsorbent. Also, the degree of ionization and speciation of metal ions has been affected by the pH (Hoslett et al., 2019). Therefore, it is necessary to optimize the pH for the metal ions adsorption process on the algae bio-char.

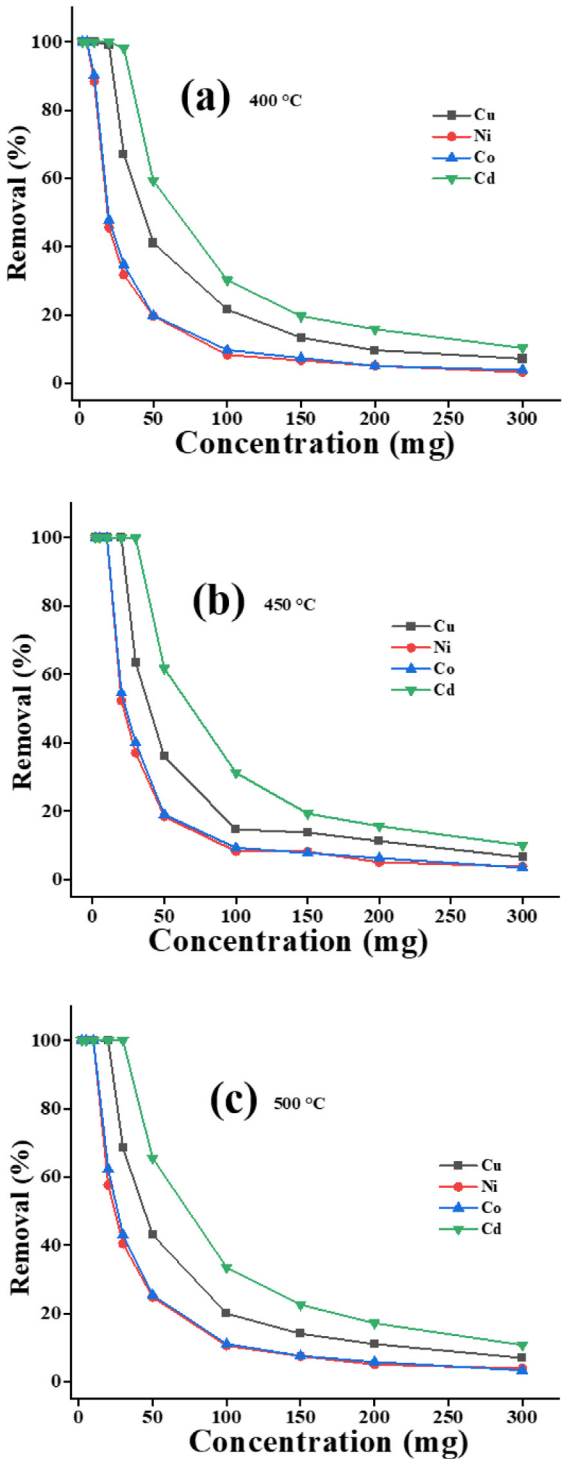

Fig. 6. Effect of initial metal ions concentration on adsorption onto biochar prepared at (a) 400 °C (b) 450 °C, and (c) 500 °C. Initial pH = 5, adsorbents dose = 250 mg/L.

The effect of pH was investigated in the range of 2.0−5.0, using a 100 ml mixture of multiple heavy metal ions (25 ml each, 25 mg/L,) with 250 mg algae bio-char (500 °C). Fig. 7 and Fig. 8S showing the results of pH effect on the adsorption capacity and removal percentage, respectively, clearly display that the adsorption capacity and removal percentage were poorest at lower pH (2.0) and increased continuously with increasing pH. At pH 2.0, the adsorption capacity and % removal

Table 7
The relative adsorption capacities of different types of bio-chars.

S. No.	Heavy metals	Type of bio-char	Adsorption capacity of heavy metals (mg/g)	References
1.	Pb^{2+}, Cu^{2+}, Cd^{2+}, and Ni^{2+}	Discarded mushroom-stick bio-char	21.0, 18.8, 11.2, and 9.8	Wang et al. (2019)
2.	Pb^{2+}, Zn^{2+}, Cu^{2+}, and Cd^{2+}	Long-root *Eichhornia crassipes* bio-char	39.09, 45.40, 48.20, and 44.04	Li et al. (2018a,b,c)
3.	Zn^{2+}	Scots pine (*Pinus sylvestris* L.) bio-char	1.07×10^{-4}	Komkiene and Baltrenaite (2016)
4.	Cu^{2+}	Silver birch (*Betula pendula*) bio-char	1.287×10^{-4}	Komkiene and Baltrenaite (2016)
5.	Pb^{2+}	Silver birch (*Betula pendula*) bio-char	1.29×10^{-6} to 3.77×10^{-6}	Komkiene and Baltrenaite (2016)
6.	Pb^{2+}	Scots pine (*Pinus sylvestris* L.) bio-char	2.37×10^{-6} to 4.49×10^{-6}	Komkiene and Baltrenaite (2016)
7.	Cu^{2+} and Cd^{2+}	Gasifier bio-char	83.7 and 68.6	(Burk et al., 2020)
8.	Cu^{2+} and Cd^{2+}	Chitosan-coated gasifier biochar	111.5 and 85.8	Burk et al. (2020)
9.	Ni^{2+}	Modified sewage sludge bio-char	35.5	Yang et al. (2019)
10.	Zn^{2+}, Cr^{2+}, Mn^{2+}, and Cu^{2+}	Sewage sludge bio-char	2.475, 8.204, 1.01, and 5.415	Zhou et al. (2017)
11.	Cu^{2+}, Ni^{2+}, Co^{2+}, and Cd^{2+}	Macroalgal bloom bio-char	10.90, 5.74, 5.80 and 16.28	This study

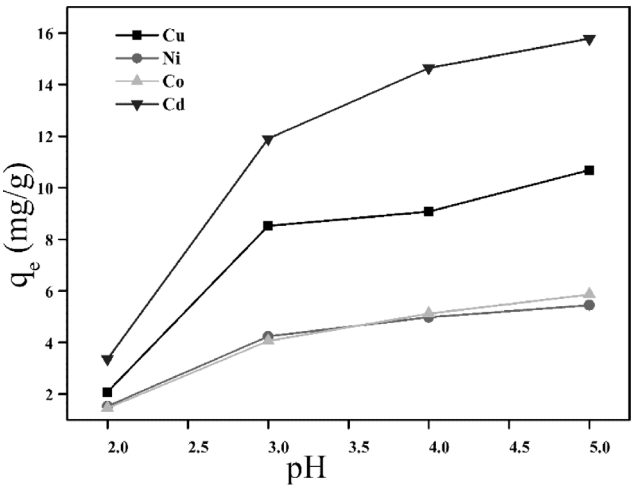

Fig. 7. Effect of pH on the adsorption capacity of algae bio-char prepared at 500 °C on multiple heavy metal ions.

for Cu (II), Ni (II), Co (II) and Cd (II) were 2.07/1.53/1.46/3.36 and 10.39/7.65/7.3/16.8, which was increased up to 10.68/5.45/5.86/15.78 and 53.40/27.25/29.3/78.9 at 5.0 solution pH, respectively. At a strong acidic condition, the surface of the algae bio-char was protonated and positively changed due to the presence of a higher concentration of H^+ ions. Thus, metal ions cannot move towards the protonated surface due to electrostatic repulsion of the same charges and hence found lower adsorption capacity at low pH (Xiao et al., 2017; Zhang et al., 2020). Also, triggers competition occurs between the heavy metal ions and hydrogen ions for adsorption sites which leads to low adsorption capacities. As the solution pH increased, the adsorption sites of algae bio-char became negatively charged due to which more heavy metal ions were removed. Also, with increasing solution pH, competition between heavy metal ions and hydrogen ions is decreased, resulting in an increase in the adsorption capacity of heavy metal ions. The point of the zero charge (P_{zpc}) of algae bio-char was less than 2.6 as recently reported by our research group (Jaiswal et al., 2021) due to which surface of the algae bio-char become deprotonated above this value ($pH>P_{zpc}$), thereby electrostatic attraction between the surface of MB-OB and MB-DOB and heavy metal ions increased which help in the removal of heavy metals from water. At the pH above 5, the white precipitate of the cadmium hydroxide was formed due to which the initial concentration of metal ions decreased (Park et al., 2017) and affected the adsorption capacity and removal percentage. Based on the above discussion, the pH effect was investigated in the range of 2.0–5.0 and pH 5.0 was chosen as optimum adsorption pH for further experiments.

4. Conclusion

In this study, toxic algal bloom biomass was successfully deployed to generate bio-oil and biochar via hydropyrolysis under supercritical conditions. The hydropyrolysis temperatures play a noteworthy role in the yield and superiority of bio-oil and biochar. GC–MS study of Bio-oil exhibited that bio-oil contains mainly fatty acids, alcohols, and hydrocarbons, indicating that this can be applied as alternative fossil fuels. Carbon-based material is deliberated as efficient, operative, cheap, and ecofriendly sorbents for inorganic micropollutants. Three biochars prepared at different temperatures follow the PSO kinetics and Langmuir isotherm to adsorptive removal for Cu(II), Ni(II), Co(II), and Cd(II) metal ions from the multiple metal aqueous systems. Higher adsorption capacities 10.90, 5.74, 5.80, and 16.28 mg/g were shown by the biochar prepared at 500 °C with Cu(II), Ni(II), Co(II), and Cd(II) metal ion, respectively. So, green algal blooms can be deliberated as prospective feedstock to generate bio-oil and biochar from mixed heavy metals from wastewater and promising elucidation for the management of green algal blooms.

CRediT authorship contribution statement

Krishna Kumar Jaiswal: Methodology, Investigation, Writing - original draft. **Vinod Kumar:** Conceptualization, Supervision, Writing - review & editing. **Mikhail S. Vlaskin:** Conceptualization, Review of writing. **Manisha Nanda:** Conceptualization, Review of writing. **Monu Verma:** Conceptualization, Supervision, Writing - review & editing. **Waseem Ahmad:** Methodology, Investigation. **Hyunook Kim:** Conceptualization, Supervision, Writing - review & editing.

Declaration of competing interest

The authors declare that they have no known competing financial interests or personal relationships that could have appeared to influence the work reported in this paper.

Acknowledgments

Financial assistance was provided by the DST, Govt. of India (Indo Russian research project INT/RUS/RFBR/347). Also, this work was supported by the Brain Pool Program through the National Research Foundation of Korea (NRF) funded by the Ministry of Science and ICT (2019H1D3A1A01102657).
This paper has been supported by the RUDN University Strategic Academic Leadership Program.

Appendix A. Supplementary data

Supplementary material related to this article can be found online at https://doi.org/10.1016/j.eti.2021.101440.

References

Arora, N., Jaiswal, K.K., Kumar, V., Vlaskin, M.S., Nanda, M., Pruthi, V., Chauhan, P.K., 2020. Small-scale phyco-mitigation of raw urban wastewater integrated with biodiesel production and its utilization for aquaculture. Bioresour. Technol. 297, 122489.
Bird, M., Wurster, C.M., De Paula Silva, P.H., Bass, A.M., De Nys, R., 2011. Algal biochar-production and properties. Bioresour. Technol. 102, 1886–1891.
Burk, G.A., Herath, A., Crisler I.I., G.B., Bridges, D., Patel, S., Pittman Jr, C.U., Mlsna, T., 2020. Cadmium and copper removal from aqueous solutions using chitosan-coated gasifier biochar. Front. Environ. Sci. 8, 541203.
Carolin, C.F., Kumar, P.S., Saravanan, A., Joshiba, G.J., Naushad, M., 2017. Efficient techniques for the removal of toxic heavy metals from aquatic environment: A review. J. Environ. Chem. Eng. 5 (3), 2782–2799.
Chen, T., Zhang, Y., Wang, H., Lu, W., Zhou, Z., Zhang, Y., Ren, L., 2014a. Influence of pyrolysis temperature on characteristics and heavy metal adsorptive performance of biochar derived from municipal sewage sludge. Bioresour. Technol. 164, 47–54.
Chen, W.T., Zhang, Y., Zhang, J., Yu, G., Schideman, L.C., Zhang, P., Minarick, M., 2014b. Hydrothermal liquefaction of mixed-culture algal biomass from wastewater treatment system into bio-crude oil. Bioresour. Technol. 152, 130–139.
Chiaramonti, D., Prussi, M., Buffi, M., Rizzo, A.M., Pari, L., 2017. Review and experimental study on pyrolysis and hydrothermal liquefaction of microalgae for biofuel production. Appl. Energy 185, 963–972.
Choudhary, P., Malik, A., Pant, K.K., 2017. Mass-scale algal biomass production using algal biofilm reactor and conversion to energy and chemical precursors by hydropyrolysis. ACS Sustain. Chem. Eng. 5 (5), 4234–4242.
Cole, A.J., Paul, N.A., De Nys, R., Roberts, D.A., 2017. Good for sewage treatment and good for agriculture: Algal based compost and biochar. J. Environ. Manage. 200, 105–113.
Dai, Z., Meng, J., Muhammad, N., Liu, X., Wang, H., He, Y., et al., 2013. The potential feasibility for soil improvement, based on the properties of biochars pyrolyzed from different feedstocks. J. Soils Sediments 13 (6), 989–1000.
De Bhowmick, G., Sarmah, A.K., Sen, R., 2018. Production and characterization of a value added biochar mix using seaweed, rice husk and pine sawdust: a parametric study. J. Cleaner Prod. 200, 641–656.
Demirbas, A., Fatih, M., 2010. Algae As a New Source of Biodiesel. Springer, London, UK.
Fan, C., Yan, J., Huang, Y., Han, X., Jiang, X., 2015. XRD and TG-FTIR study of the effect of mineral matrix on the pyrolysis and combustion of organic matter in shale char. Fuel 139, 502–510.
Freundlich, H., 1907. Über die adsorption in lösungen. Z. Phys. Chem. 57 (1), 385–470.
Fu, F., Wang, Q., 2011. Removal of heavy metal ions from wastewaters: a review. J. Environ. Manage. 92 (3), 407–418.
Garcia Alba, L., Torri, C., Samorì, C., van der Spek, J., Fabbri, D., Kersten, S.R., Brilman, D.W., 2012. Hydrothermal treatment (HTT) of microalgae: evaluation of the process as conversion method in an algae biorefinery concept. Energy Fuels 26 (1), 642–657.

Gupta, V.K., Nayak, A., Agarwal, S., 2015. Bioadsorbents for remediation of heavy metals: current status and their future prospects. Environ. Eng. Res. 20 (1), 1–18.
He, H.J., Xiang, Z.H., Chen, X.J., Chen, H., Huang, H., Wen, M., Yang, C.P., 2018. Biosorption of Cd(II) from synthetic wastewater using dry biofilms from biotrickling filters. Int. J. Environ. Sci. Technol. 15, 1491–1500.
Hoslett, J., Ghazal, H., Ahmad, D., Jouhara, H., 2019. Removal of copper ions from aqueous solution using low temperature biochar derived from the pyrolysis of municipal solid waste. Sci. Total Environ. 673, 777–789.
Hossain, M.K., Strezov, V., Chan, K.Y., Ziolkowski, A., Nelson, P.F., 2011. Influence of pyrolysis temperature on production and nutrient properties of wastewater sludge biochar. J. Environ. Manage. 92 (1), 223–228.
Jaiswal, K.K., Kumar, V., Verma, R., Verma, M., Kumar, A., Vlaskin, M.S., Nanda, M., Kim, H., 2021. Graphitic bio-char and bio-oil synthesis via hydrothermal carbonization-co-liquefaction of microalgae biomass (oiled/de-oiled) and multiple heavy metals remediations. J. Hard Mater. 409, 124987.
Jena, U., Das, K.C., Kastner, J.R., 2012. Comparison of the effects of Na2CO3, Ca3(PO4)2, and NiO catalysts on the thermochemical liquefaction of microalga Spirulina platensis. Appl. Energy 98, 368–375.
Jung, K.W., Hwang, M.J., Jeong, T.U., Ahn, K.H., 2015. A novel approach for preparation of modified-biochar derived from marine macroalgae: dual purpose electro-modification for improvement of surface area and metal impregnation. Bioresour. Technol. 191, 342–345.
Jung, C., Park, J., Lim, K.H., Park, S., Heo, J., Her, N., et al., 2013. Adsorption of selected endocrine disrupting compounds and pharmaceuticals on activated biochars. J. Hard Mater. 263, 702–710.
Komkiene, J., Baltrenaite, E., 2016. Biochar as adsorbent for removal of heavy metal ions [Cadmium (II), Copper (II), Lead (II), Zinc (II)] from aqueous phase. Int. J. Environ. Sci. Technol. 13, 471–482.
Kumar, V., Kumar, S., Chauhan, P.K., Verma, M., Bahuguna, V., Joshi, H.C., Ahmad, W., Negi, P., Sharma, N., Ramola, B., Rautela, I., 2019. Low-temperature catalyst based hydrothermal liquefaction of harmful macroalgal blooms, and aqueous phase nutrient recycling by microalgae. Sci. Rep. 9, 1–9.
Kumar, V., Nanda, M., 2016. Biomass pyrolysis-current status and future directions. Energy Sources A 38, 2914–2921.
Lam, S.S., Russell, A.D., Lee, C.L., Lam, S.K., Chase, H.A., 2012. Production of hydrogen and light hydrocarbons as a potential gaseous fuel from microwave-heated pyrolysis of waste automotive engine oil. Int. J. Hydrogen Energy 37 (6), 5011–5021.
Li, R., Deng, H., Zhang, X., Wang, J.J., Awasthi, M.K., Wang, Q., Xiao, R., Zhou, B., Du, J., Zhang, Z., 2019. High-efficiency removal of Pb (II) and humate by a CeO2–MoS2 hybrid magnetic biochar. Bioresour. Technol. 273, 335–340.
Li, H., Mahyoub, S.A.A., Liao, W., Xia, S., Zhao, H., Guo, M., Ma, P., 2017. Effect of pyrolysis temperature on characteristics and aromatic contaminants adsorption behavior of magnetic biochar derived from pyrolysis oil distillation residue. Bioresour. Technol. 223, 20–26.
Li, Q., Tang, L., Hu, J., Jiang, M., Shi, X., Zhang, T., Li, Y., Pan, X., 2018a. Removal of toxic metals from aqueous solution by biochars derived from long-root Eichhornia crassipes. Roy. Soc. Open Sci. 5, 180966.
Li, R., Wang, J.J., Gaston, L.A., Zhou, B., Li, M., Xiao, R., Wang, Q., Zhang, Z., Huang, H., Liang, W., Huang, H., 2018b. An overview of carbothermal synthesis of metal–biochar composites for the removal of oxyanion contaminants from aqueous solution. Carbon 129, 674–687.
Li, X., Wu, S., Yang, C., Zeng, G., 2020a. Microalgal and duckweed based constructed wetlands for swine wastewater treatment: A review. Bioresour. Technol. 318, 123858.
Li, X., Yang, W.L., He, H., Wu, S., Zhou, Q., Yang, C., Zeng, G., Luo, L., Lou, W., 2018c. Responses of microalgae coelastrella sp. to stress of cupric ions in treatment of anaerobically digested swine wastewater. Bioresour. Technol. 251, 274–279.
Li, X., Yang, C., Zeng, G., Wu, S., Lin, Y., Zhou, Q., Lou, W., Du, C., Nie, L., Zhong, Y., 2020b. Nutrient removal from swine wastewater with growing microalgae at various zinc concentrations. Algal Res. 46, 101804.
Li, R., Zhang, Y., Deng, H., Zhang, Z., Wang, J.J., Shaheen, S.M., Xiao, R., Rinklebe, J., Xi, B., He, X., Du, J., 2020c. Removing tetracycline and Hg (II) with ball-milled magnetic nanobiochar and its potential on polluted irrigation water reclamation. J. Hazard. Mater. 384, 121095.
Maliutina, K., Tahmasebi, A., Yu, J., 2018. Effects of pressure on morphology and structure of bio-char from pressurized entrained-flow pyrolysis of microalgae. Data Brief 18, 422–431.
McDonald-Wharry, J., Manley-Harris, M., Pickering, K., 2013. Carbonisation of biomass-derived chars and the thermal reduction of a graphene oxide sample studied using Raman spectroscopy. Carbon 59, 383–405.
Merceron, M., Antoine, V., Auby, I., Mor, P., 2007. In situ growth potential of the subtidal part of green-tide forming *Ulva spp.* Stocks. Sci. Total Environ. 384, 293–305.
Morand, P., Merceron, M., 2005. Macroalgal population and sustainability. J. Coast. Res. 21, 1009–1020.
N'Yeurt, A.D.R., Iese, V., 2015. The proliferating brown alga Sargassum polycystum in Tuvalu, South Pacific: assessment of the bloom and applications to local agriculture and sustainable energy. J. Appl. Phycol. 27 (5), 2037–2045.
Park, C.M., Han, J., Chu, K.H., Al-Hamadani, Y.A., Her, N., Heo, J., Yoon, Y., 2017. Influence of solution pH. ionic strength, and humic acid on cadmium adsorption onto activated biochar: experiment and modeling. J. Ind. Eng. Chem. 48, 186–193.
Park, D., Yun, Y.S., Park, J.M., 2010. The past, present, and future trends of biosorption. Biotechnol. Bioprocess. Eng. 15 (1), 86–102.
Ren, J., Zhao, Z., Ali, A., Guan, W., Xiao, R., Wang, J.J., Ma, S., Guo, D., Zhou, B., Zhang, Z., Li, R., 2020. Characterization of phosphorus engineered biochar and its impact on immobilization of Cd and Pb from smelting contaminated soils. J. Soils Sediments 20, 3041–3052.
Rhim, Y.R., Zhang, D., Fairbrother, D.H., Wepasnick, K.A., Livi, K.J., Bodnar, R.J., Nagle, D.C., 2010. Changes in electrical and microstructural properties of microcrystalline cellulose as function of carbonization temperature. Carbon 48 (4), 1012–1024.
Ross, A.B., Biller, P., Kubacki, M.L., Li, H., Lea-Langton, A., Jones, J.M., 2010. Hydrothermal processing of microalgae using alkali and organic acids. Fuel 89 (9), 2234–2243.
Selvanathan, M., Yann, K.T., Chung, C.H., Selvarajoo, A., Arumugasamy, S.K., Sethu, V., 2017. Adsorption of copper (II) ion from aqueous solution using biochar derived from rambutan (nepheliumlappaceum) peel: feedforward neural network modelling study. Water Air Soil Pollut. 228 (8), 299.
Shakya, R., Whelen, J., Adhikari, S., Mahadevan, R., Neupane, S., 2015. Effect of temperature and Na_2CO_3 catalyst on hydrothermal liquefaction of algae. Algal Res. 12, 80–90.
Subedi, R., Taupe, N., Pelissetti, S., Petruzzelli, L., Bertora, C., Leahy, J.J., Grignani, C., 2016. Greenhouse gas emissions and soil properties following amendment with manure-derived biochars: Influence of pyrolysis temperature and feedstock type. J. Environ. Manag. 166, 73–83.
Verma, M., Kumar, A., Singh, K.P., Kumar, R., Kumar, V., Srivastava, C.M., et al., 2020. Graphene oxide-manganese ferrite (GO-MnFe2O4) nanocomposite: One-pot hydrothermal synthesis and its use for adsorptive removal of Pb2+ ions from aqueous medium. J. Molecular Liquids 315, 113769.
Verma, M., Tyagi, I., Chandra, R., Gupta, V.K., 2017. Adsorptive removal of Pb (II) ions from aqueous solution using cuo nanoparticles synthesized by sputtering method. J. Molecular Liquids 225, 936–944.
Wang, J., Chen, C., 2009. Biosorbents for heavy metals removal and their future. Biotechnol. Adv. 27 (2), 195–226.
Wang, X., Li, X., Liu, G., He, Y., Chen, C., Liu, X., Li, G., Gu, Y., Zhao, Y., 2019. Mixed heavy metal removal from wastewater by using discarded mushroom-stick biochar: Adsorption properties and mechanisms. Environ. Sci. Processes Impacts 21, 584–592.
Xiao, Y., Xue, Y., Gao, F., Mosa, A., 2017. Sorption of heavy metal ions onto crayfish shell biochar: effect of pyrolysis temperature, pH and ionic strength. J. Taiwan Instit. Chem. Eng. 80, 114–121.
Yang, L., He, L., Xue, J., Wu, L., Ma, Y., Li, H., Peng, P., Li, M., Zhang, Z., 2019. Highly efficient nickel (II) removal by sewage sludge biochar supported α-Fe2O3 and α-FeOOH: Sorption characteristics and mechanisms. PLoS One 14, e0218114.

Yu, K.L., Lau, B.F., Show, P.L., Ong, H.C., Ling, T.C., Chen, W.H., Ng, E.P., Chang, J.S., 2017. Recent developments on algal biochar production and characterization. Bioresour. Technol. 246, 2–11.
Zhang, H., Xu, F., Xue, J., Chen, S., Wang, J., Yang, Y., 2020. Enhanced removal of heavy metal ions from aqueous solution using manganese dioxide-loaded biochar: Behavior and mechanism. Sci. Rep. 10, 1–3.
Zhao, J., Shen, X.J., Domene, X., Alcañiz, J.M., Liao, X., Palet, C., 2019. Comparison of biochars derived from different types of feedstock and their potential for heavy metal removal in multiple-metal solutions. Sci. Rep. 9 (1), 1–12.
Zhou, L., Jia, Y., Nguyen, T.H., Adesina, A.A., Liu, Z., 2013. Hydropyrolysis characteristics and kinetics of potassium-impregnated pine wood. Fuel Process. Technol. 116, 149–157.
Zhou, D., Liu, D., Gao, F., Li, M., Luo, X., 2017. Effects of biochar-derived sewage sludge on heavy metal adsorption and immobilization in soils. Int. J. Environ. Res. Publ. Health 14 (681).